A MODEL TO PREDICT THE SHORT-TERM TURBULENT INDOOR DISPERSION OF SMALL DROPLETS AND DROPLET NUCLEI RELEASED FROM COUGHS AND SNEEZES

Jordi Pallares*, Alexandre Fabregat

Departament d'Enginyeria Mecànica. Universitat Rovira i Virgili. Tarragona. Spain

*Corresponding author: jordi.pallares@urv.cat

Keywords: indoor dispersion, cough, sneeze, turbulent jet, turbulent puff, unsteady jet

ABSTRACT

We propose a simple model to predict the short-term indoor turbulent dispersion of the aerosol cloud produced by violent expiratory events. Once the air injection ceases, the turbulent jet transitions to a thermal puff that progressively decays due to viscous effects. According to recent literature, the expelled liquid droplets of saliva and sputum smaller than 20-30 μm in diameter stay afloat within this decaying turbulent puff. In contrast, droplets larger than 100 μm tend to leave the puff following quasi-ballistic trajectories and landing on the floor at relatively short times after release. The model presented here is capable of providing good estimates for the shape and dimensions of the cloud composed of the lighter fraction of droplets as a function of the intensity and the duration of the flow injection and the density difference between the exhaled and the ambient air. Predictions agree with Direct Numerical Simulations and experiments reported in the literature. This model can be used as an operational tool to determine the short-term spatial range of expelled droplets and provides realistic initial conditions for simulations of long-term dispersion of pathogen-laden clouds in indoor environments with forced and natural ventilation.

INTRODUCTION

The contact or the inhalation of aerosols expelled from infected subjects while talking, laughing, singing, during intense breathing or when coughing and sneezing is considered one of the major routes of transmission of COVID-19 as well as other infectious diseases caused by viruses and bacteria such as the human H1N1 flu, the bird flu (H5N1), the SARS or the tuberculosis.[1-3] Consequently, it is clear that the analysis of processes of generation, emission and dispersion of aerosols is key, on one hand, to understand the transmission of pathogens of these known diseases and, probably, of others that will appear in the future and on the other hand, to design effective protection, containment and social distancing measures based on scientific evidence.[4]

Violent expiratory events, as coughing and sneezing, are recognized as an important vector of infection because of the large number of aerosol particles expelled in these events with a relatively large velocity that reach relatively large distances.[5] Another key aspect in the dispersion of aerosols is the diameter of the expelled individual droplets of saliva and sputum. Large liquid particles, with large Stokes number, will follow quasi-ballistic trajectories independently of the generated background turbulent flow, while smaller particles, with small Stokes numbers and small settling velocities, will be advected by the flow and may stay afloat for longer times than the larger particles.[6] In addition, the initial expelled diameter of the liquid droplet can change due to evaporation depending on the differences of temperature and humidity between the exhaled air and the ambient condition.[7] It has been estimated that once the water portion of the saliva and sputum droplets has been evaporated the diameter of the small remaining droplet nuclei is approximately between one half[8] and one third[9] of the initial droplet diameter. This reduction of the diameter of droplets could enhance the chance of particles to remain afloat within the exhaled cloud for longer times.

The flow generated by unsteady injections of buoyant or non-buoyant fluids into quiescent or stratified environments has attracted attention because of implications in atmospheric pollution, environmental flows,[10] intraventricular blood flows,[11] propulsion of aquatic animals[12] and in technological and industrial applications of jet flows, such as internal combustion engines, gas turbine combustors and spray dryers.[13] The analysis of these flows in connection to the analysis of the spread of infectious diseases via the aerial transmission is more recent and it has experienced a rapid growth during the ongoing COVID-19 pandemic.[3]

The characteristics of the exhaled flow in coughs and sneezes has been analyzed experimentally to determine the typical duration of the event, the magnitude and the orientation of the discharged air velocity, the typical areas and shapes of the mouth exit and the temperature and humidity conditions of the exhaled flow.[14-16] The number, size distributions,[17-20] composition[21,8,9] and properties of expelled droplets have been also determined experimentally. This information has been important to establish experimental conditions in synthetic experiments with scale models in water tanks[5] and with mannequins,[22,23] as well as to impose realistic boundary conditions in numerical simulations.

Authors	Application/ Space	Computational domain (m^3)	Volume (m^3)	Mesh elements ($x10^6$)	Turbulence	Particles	Simulation code
Gupta et al. [24]	Aircraft cabin	4.1 x 5.3 x 2.0*	43	1.5	RANS k-ω	Lagrangian	Ansys Fluent
Thatiparti et al.[25]	Isolation room	4.3 x 4.9 x 2.4	51	1.6	RANS k-ε	Lagrangian	Ansys Fluent
Yang et al.[26]	Airliner cabin section	1 x 1.77 x 2.19*	3.9*	1.9	RANS k-ε	Lagrangian	Ansys CFX
Nazari et al.[27]	Parking	122 x 86 x 2.9	30000	0.7	RANS k-ω	Lagrangian	OpenFoam
Yu et al.[28]	Office	4.3 x 3.1 x 2.7	36	1.5	RANS k-ε	Lagrangian	Ansys Fluent
Dbouk & Drikakis[29]	Parallepipedic volume	6 x 1 x 3	18	0.5	RANS k-ω	Lagrangian	OpenFoam
Diwan et al. [30]	Parallepipedic volume	1 x 2 x 1	2.0	2100	DNS	-	In-house code
Pendar & Páscoa[31]	Room	4 x 3 x 3	36	5.1	LES	Lagrangian	OpenFoam
Shao and Li[32]	Hall	20 x 20 x 12	4800	0.6	RANS	Convection diffusion	In-house code
Zhang et al.[33]	Urban bus	12.1 x 2.58 x 2.95**	57	5.9	RANS	Convection-diffusion	OpenFoam
Dbouk & Drikakis[34]	Elevator	1.24 x 1 x 2.2	2.7	0.6	RANS k-ω	Lagrangian	OpenFoam
Liu et al.[35]	Restaurant	17.5 x 8.3 x 3.14	460	8.0	LES	Lagrangian	In-house code
Fontes et al.[36]	Room	Vertical cylinder (R=3 m, H=3 m)	85	2.4	DES	Lagrangian	Star CCM+
Fabregat et al.[6]	Cylindrical volume	Horizontal cylinder (R = 0.5 m, H = 1.6 m)	1.3	370	DNS	Lagrangian	Nek5000
Foster and Kinzel[37]	Classroom	9.5 x 7 x 2.7	66	1.9	DES	Convection	Star CCM+
Cravero and Marsano[38]	Room	5 x 3 x 3 3.5 x 3 x 2.5	45 26	2.0 2.6	RANS k-ε	Lagrangian	Ansys CFX
Abkarian et al.[39]	Sphere	Radius = 3 m	14.1	17.7	LES	Lagrangian	In-house code
Wang et al. [40]	Cylindrical volume	Horizontal cylinder (R = 1.5 m, H = 3 m)	21.2	21.9	LES	Lagrangian	In-house code

* estimated, ** bus dimensions

Table I. Characteristics of CFD studies of particle/contaminant dispersion in confined spaces

The number of papers reporting numerical simulations of the turbulent flow associated with intense or violent expiratory events has raised significantly during 2020 with the outbreak of the pandemic COVID-19 as a step forward to gain understanding on the virus laden-particle dispersion. Table I shows, as an example, a non-exhaustive list of numerical studies using different strategies for the modelization of the turbulent flow that range from relatively simple parametrization of the turbulence, based on the solution of the Reynolds-Averaged Navier

Stokes equations (RANS), spatially filtered Large-Eddy Simulation technique (LES), RANS-LES hybrid techniques including Detached-Eddy Simulation (DES), to the Direct Numerical Simulation (DNS) of the flow. The computational cost of the RANS simulations varies considerably depending on the grid size and the treatment of the flow transient nature, either steady (RANS) or time varying (URANS). A typical simulation may require around a few thousands of CPU hours.[34] LES and DNS are far more expensive with about some hundreds of thousands of CPU hours.[6,30] Table I also indicates the physical situation considered in each study, the size of the computational domain and the number of mesh elements used. Most of the studies indicated in Table I include computational grids that resolve the exit geometry of the mouth with elements sizes in the range of a few millimeters in this region and significantly coarser grid in the far field. This grid strategy aims to capture both the relatively fast flow injection, produced by a cough or a sneeze, and the subsequent aerosol cloud dispersion, within relatively large, confined spaces (see Table I), caused, in most of these cases, by some forced or natural convection background flow. However, these two sequential processes have quite different time scales. While the flow generated in coughs and sneezes has a time scale of a few seconds, with flow injections lasting for less than a second,[14] the background flow, with typical velocities of 0.1-0.2 m/s in ventilated spaces with dimensions of a few or several metres can have time scales of the order of tens or hundreds of seconds.

In this study we present and validate a model to predict the short-term dispersion of the aerosol cloud composed of small droplets and droplet-nuclei expelled in violent expiratory events. We propose a simple way to determine the envelope of the terminal shape of the aerosol cloud after a few seconds of the onset depending on the intensity and duration of the flow injection and the density difference between the exhaled and ambient air. This cloud geometry can be used to establish specific short-term safety distances and to impose initial conditions for long-term simulations of the cloud dispersion within forced or natural ventilated spaces. This strategy can alleviate the computational requirements of these simulations, which usually are oriented towards the determination of the dispersion of small droplets and droplets nuclei, that stay afloat for long times, for specific environments with specific ventilation conditions. In this paper we describe the theoretical basis of the model and compare predictions of the model with experiments and numerical simulations

THEORETICAL MODELS

The turbulent flow generated in a typical violent expiratory event can be understood as a quasi-horizontal short intense injection of a relatively hot and moist air, with density ρ_d, into the ambient, with density ρ_a. During the injection a turbulent starting jet develops. Flow visualizations in water tanks of this stage reveal the progressive axial advance of the jet tip and the simultaneous increase of the radius of the jet, as those shown in Fig. 6 of Richards[41], in Fig. 10 of Bourouiba et al.[5] or animations of positions of small particles, with very small inertia, from DNS reported by Fabregat et al.[6] This dynamic can be understood as the progressive growth of the height and the maximum radius of a conical-shaped cloud. Once the discharge has finished, the head of the jet tip progressively detaches from the conical cloud forming a puff that, eventually, can be further displaced along the vertical direction because of buoyancy. In this stage, when the flow injection has ceased, rates of axial advance and of the radius growth of the conical cloud start to decrease and the puff progressively decelerates

until both the conical cloud and the frontal puff attain residual velocities. Figure 1 shows a sketch of this quasi-terminal shape of the cloud generated by the flow discharge, with density ρ_d, into a quiescent ambient with a different density ρ_a with $\rho_a > \rho_d$. This buoyancy effect produces different rates of entrainment along the vertical and horizontal directions and, consequently, different vertical and horizontal diameters of the cloud (D_{cv} and D_{ch}, respectively, as indicated in Fig. 1b). The envelope of this final topology can be divided into a tronco-conical volume, with an ellipsoidal cross section, and a frontal quasi-spherical volume, with radius R_p and centre at (x_p, y_p). These two volumes are connected through a neck located at an axial distance from the jet exit of x_n (see Fig. 1).

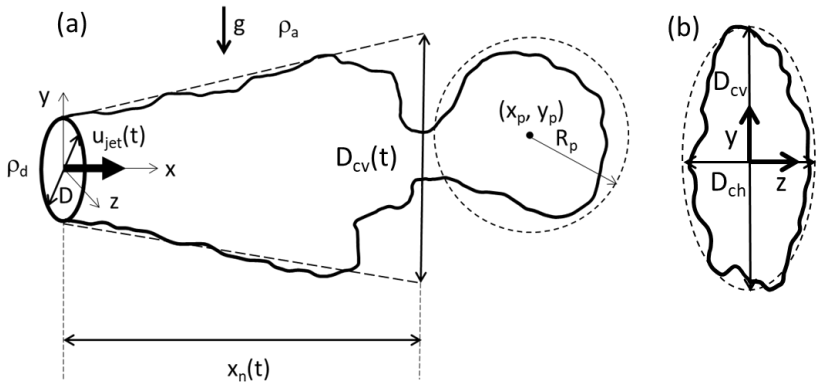

Figure 1. Sketch of the cloud generated in a violent expiratory event. (a) Lateral view. (b) Frontal view.

The transient nature of the velocity of the air expelled during a cough or a sneeze can be modelled with a time evolution that ramps up from zero to the maximum velocity ($u_{jet,max}$) at time ($t_{u_{max}}$) and then linearly decays back to zero at time (t_j). This model for the jet velocity can be written as equation (1).

$$u_{jet}(t) = \begin{cases} \frac{u_{jet,max}}{t_{u_{max}}} t & 0 \le t < t_{u_{max}} \\ u_{jet,max} - \frac{u_{jet,max}}{t_j - t_{u_{max}}} \left(t - t_{u_{max}}\right) & t_{u_{max}} \le t \le t_j \\ 0 & t > t_j. \end{cases} \quad (1)$$

According to experimental measurements of coughs[14] there is a wide variability of three parameters. Typical values of $u_{jet,max}$ range approximately between 4 m/s to 20 m/s, $t_{u_{max}}$ from 0.06 s to 0.15 s and t_j from 0.3 to 0.6 s. Once the injection has finished the velocity of the expelled puff decreases as[10] $U_p \sim t^{-3/4}$ reaching the typical background velocities in ventilated spaces of 0.1-0.2 m/s within the range of one to four seconds depending on the intensity and duration of the violent expiratory event. After this initial period of time the transport and dispersion of the expelled cloud will be dominated by the ambient currents.

Modelization of the cloud shape with the effective jet velocity.

For a jet with a constant injection (U_{inj}) the velocity decay at the centreline in the self-similarity region can be written as equation (2).[13, 42]

$$U(x) = \frac{dx}{dt} = \frac{3\,U_{inj}\,D}{K\,x} \quad \text{for } x \geq x_0, \tag{2}$$

where K is the entrainment constant, D is the diameter of the jet and x_0 is the position of the jet exit with respect to the virtual origin. For a starting jet with a constant injection velocity, x in Eq. (2) can be understood as the jet tip position. Integrating Eq. 2, this position as a function of time can be expressed as equation (3).

$$x(t) = \left(\frac{6U_{inj}D\,t}{K}\right)^{1/2}, \tag{3}$$

For a jet with an injection velocity changing in time Abani and Reitz[43] developed a model to compute the effective injection velocity perceived by the jet tip. This effective injection velocity can be used in Eq. (2) to determine the jet tip penetration, x. According to Abani and Reitz[43] this effective injection velocity for a starting jet ($u_{jet}(t=0)=0$) with a time varying injection velocity ($u_{jet}(t)$) can be computed as equation (4).

$$U_{inj,eff}(x,t) = \int_0^t \left\{1 - exp\left[-\frac{(t-\tau)\,u_{jet}(\tau)}{St\,x}\right]\right\}\left(\frac{du_{jet}(\tau)}{d\tau}\right) d\tau. \tag{4}$$

In Eq. (4), $\frac{u_{jet}(\tau)}{St\,x}$ represents the momentum response time (t_r) for the eddy at the tip of the jet, located at x, needed to adjust to the instantaneous injection velocity occurred at time τ. This time is associated with a Strouhal number St, which relates this response time with the characteristic time of the flow, which in the jet is $\frac{x}{u_{jet}}$ (i.e., $St = \frac{u_{jet}}{x\,t_r}$). The term between braces in Eq. 4 accounts for the exponentially decaying response of the past injection jet velocity $u_{jet}(\tau)$, occurred at the earlier time τ, at the jet tip located at x at time t.

Similarly to Eq. (2), the position of the tip can be computed as equation (5).

$$\frac{dx}{dt} = \frac{3U_{inj,eff}(x,t)D}{K\,x}. \tag{5}$$

The integral of Eq. 4 can be computed numerically using a known time evolution of the injection velocity, $u_{jet}(t)$, as that indicated in Eq. 1. This model has two parameters: the entrainment constant with a value of $K = 0.457$ according to Schlichting and Gersten[42] and the Strouhal number. Abani and Reitz[43] reported that predictions with $St = 3$ reproduced well their numerical simulations of jet flows for various injection configurations. The values of the entrainment constant reported in the literature were reviewed by Abraham[13] who reported typical values in the range $0.2 \leq K \leq 0.457$.

Modelization of the puff trajectory and volume

The flow generated in coughs and sneezes can be understood as an initial turbulent jet that lasts for relatively short periods of injection times ($0 \leq t \leq t_j$) at an average velocity $\overline{u}_{jet}$. When the flow injection ends, the jet evolves to a turbulent puff for $t > t_j$. Chaudhuri et al.[44] used analytical expressions for the axial location x, axial velocity U and radial spread R for transient turbulent jets and puffs to model the puff trajectory and volume after a violent expiratory event. Neglecting the buoyancy effect, expressions for the jet flow are as described by equations (6) – (8).[13,44]

$$x_j(t) = \left(\frac{6\,\bar{u}_{jet}\,D\,t}{K}\right)^{1/2}, \tag{6}$$

$$U_j(t) = \frac{3\,\bar{u}_{jet}\,D}{K\,x_j(t)}, \tag{7}$$

$$R_j(t) = R_0 + \frac{x_j(t) - x_{j0}}{n_j}. \tag{8}$$

In Eqs. 6-8, K is the entrainment coefficient ($0.2 \leq K \leq 0.457$[13]), $n_j = 1/\tan\alpha_j$ is a constant related with the angle of spread for jets[10] ($\alpha_j \approx 11.3°, n_j \approx 5$) and x_{j0} is the position of the circular nozzle tip, of radius $R_0 = D/2$, with respect to the virtual origin of the jet ($x_{j0} = D/2\tan\alpha_j$).

According to Scorer,[10] for the puff stage (i.e. for $t > t_j$), equations (9) – (11) describe the time evolution of the position at the centre of the puff, x_p , its velocity U_p and its radius R_p.

$$x_p(t) = \left(4\,U_{p0}\,x_{po}^3\,t\right)^{1/4}, \tag{9}$$

$$U_p(t) = U_{p0}\left(\frac{x_{p0}}{x_p(t)}\right)^3, \tag{10}$$

$$R_p(t) = \frac{x_p(t)}{n_p}, \tag{11}$$

where, similarly to n_j, $n_p = 1/\tan\alpha_p$ and for puffs[10] $1.7 \leq n_p \leq 6.3$. In Eqs. 9 and 10, x_{p0} is the initial position of the puff ($x_{p0} = x_j(t_j)$). Similarly, in Eq. 11, $U_{p0} = U_j(t_j)$.

Richards[45,41] proposed a model to predict the trajectory and the volume of a buoyant puff with constant buoyancy. Bourouiba et al.[5] extended this original model to incorporate the variation of the density of the cloud and the influence of the number of aerosol particles within the cloud. This extension of the model, that neglects the contribution of the aerosol particles to buoyancy, was used by Renzi and Clarke[46] to model the properties of buoyant puffs generated in intense expiratory events. Here we adopt the same assumption considering the very low volume fraction ($\approx 10^{-5}$) of the liquid aerosol within the initial expelled puff generated in coughs and sneezes.[17] The model reduces to a set of five ordinary differential equations for the time evolution of the volume of the puff V (equation (12)), the density of the puff ρ_p (equation (13)), the buoyancy B (equation (14)), the vertical momentum I_y (equation (15)) and the distance travelled by the puff along its curvilinear trajectory s(equation (16)).

$$\frac{dV}{dt} = 3\eta\alpha^3 s^2 \frac{ds}{dt}, \tag{12}$$

$$\frac{d\rho_p}{dt} = \frac{1}{V}\frac{dV}{dt}\left(\rho_a - \rho_p\right), \tag{13}$$

$$\frac{dB}{dt} = g\rho_a\frac{dV}{dt} - g\frac{d(V\rho_p)}{dt}, \tag{14}$$

$$\frac{dI_y}{dt} = B, \tag{15}$$

$$\frac{ds}{dt} = \frac{\sqrt{I_y^2 + (I_{y0}\cos\theta_0)^2}}{V\rho_p}. \tag{16}$$

Setting the discharge angle to $\theta_0 = 0$ (horizontal injection), the initial conditions are at $t = 0$, $V = V_0$, $\rho_p = \rho_d$, $B = B_0 = gV_0(\rho_d - \rho_a)$, $I_y = 0$ and $s = 0$. The coordinates at the centre of the puff can be computed as equations (18) and (19).

$$\frac{dx}{ds} = \cos\theta \tag{18}$$

$$\frac{dy}{ds} = \sin\theta \tag{19}$$

where $\theta = \tan^{-1}\left(\frac{B_0 t}{I_0}\right)$, with I_0 the modulus of the initial momentum $I_0 = V_0 \rho_d \bar{u}_{jet}$. The detailed derivation of the model and examples of its application can be found in Bourouiba et al.[5] and Renzi and Clarke.[46] The model parameters are the shape factor of the puff η and the entrainment coefficient α. While $\eta = 4\pi/3$ corresponds to a spherical puff, Scorer[47] and Bourouiba et al.[5] suggested $\eta = 3$. Recent DNS[48] found larger values of about $\eta \approx 7$. The entrainment coefficient α for thermals ranges from 0.2 to 0.35 with a mean[47] of 0.25 or from 0.13 to 0.53 according to Richards.[41]

	Experiment I. Bourouiba et al.[5]	DNS. Fabregat et al.[6]
ρ_d (kg m^{-3})	999.75	1.18 ($T_d = 34°C$)
ρ_a (kg m^{-3})	1000.29	1.26 ($T_a = 15°C$)
I_0 (kg m s^{-1})	$8.86 \cdot 10^{-2}$	$8.28 \cdot 10^{-4}$
B_0 (kg m s^{-2})	$2.72 \cdot 10^{-3}$	$2.23 \cdot 10^{-4}$
D (m)	0.018*	0.02
u_{jet} (m s^{-1})	$1.007\ (0 \geq t \geq 0.375\ s)$ $0\ (t > 0.375\ s)$	$32\ t\ (0 \geq t \geq 0.15\ s)$ $-19.2\ t + 7.68\ (0.15 > t \geq 0.4\ s)$ $0\ (t > 0.4\ s)$
$u_{jet,max}$ (m s^{-1})	1.007	4.8
$Re_m = u_{jet,max} D/\nu$	$1.81 \cdot 10^{4}$*	$6.00 \cdot 10^{3}$
$Gr = g\Delta\rho D^3/\rho_0 \nu^2$	$3.09 \cdot 10^{4}$*	$2.02 \cdot 10^{4}$
$Ri = Gr/Re_m^2$	$9.40 \cdot 10^{-5}$*	$5.61 \cdot 10^{-4}$

* based on the duration, the volume and the velocity of the injection reported in Bourouiba et al.[5]

Table 2. Parameters of the experiment I of Bourouiba et al.[5] and the DNS of Fabregat et al.[6]

COMPARISON WITH EXPERIMENT AND SIMULATION

Bourouiba et al.[5] reported experiments of fluid injections with solid particles discharged in a large quiescent water tank. Table 2 summarizes conditions of the experiment, carried out without particles and labelled as Experiment I in Bourouiba et al.[5] The corresponding values of the maximum Reynolds number (Re_m), the Grashof number (Gr) and the Richardson number (Ri) are also indicated in Table 2. For this particular experiment, these authors show visualizations of the turbulent dyed buoyant cloud in their Figure 10. Conditions of the DNS by Fabregat et al.[6] are also included in Table II. These authors performed DNS of the flow generated by a pulse jet with a spectral element code and released particles with diameters 4, 8, 16, 32, 64, 128 and 256 µm during the flow injection. The one-way Lagrangian particle advection model was coupled with an evaporation model to account for the diameter reduction. The particles were divided into two groups containing all the diameters. For one

group evaporation was considered and particles could shrink down to one third of their initial diameter to emulate the formation of droplet nuclei constituted by non-evaporable residual. For the other group of particles, their diameters were kept constant (non-evaporative particles). According to Fabregat et al.[6] the overall characteristics of the cloud constituted by small particles (4, 8, 16 and 32 μm) were essentially independent of the evaporation of particles. Evaporation was found to effectively decrease the diameter of smaller particles, as reported elsewhere[47-49, 7] but the shape of the cloud of small droplets and droplets nuclei (<20-30 μm) was insensitive to the evaporation (see for example Figs. 8 and 9 in Fabregat et al.[6]

Despite the use of different working fluids (water in the experiment and air in the simulation), non-dimensional groups differences between two injections are relatively modest, both similar to typical violent expiratory events. Different time evolutions of jet velocities were observed during discharges that last approximately the same period of time (see Table 2). In the case of experiments, the flow injection was released with a piston, giving a 'top-hat' time evolution of the jet velocity, while the DNS adopted the unsteady jet velocity given in Eq. 1 with, $u_{jet,max} = 4.8\ m/s, t_{u_{max}} = 0.15\ s$ and $t_j = 0.4\ s$, and inspired in measurements of coughs performed by Gupta et al.[14]

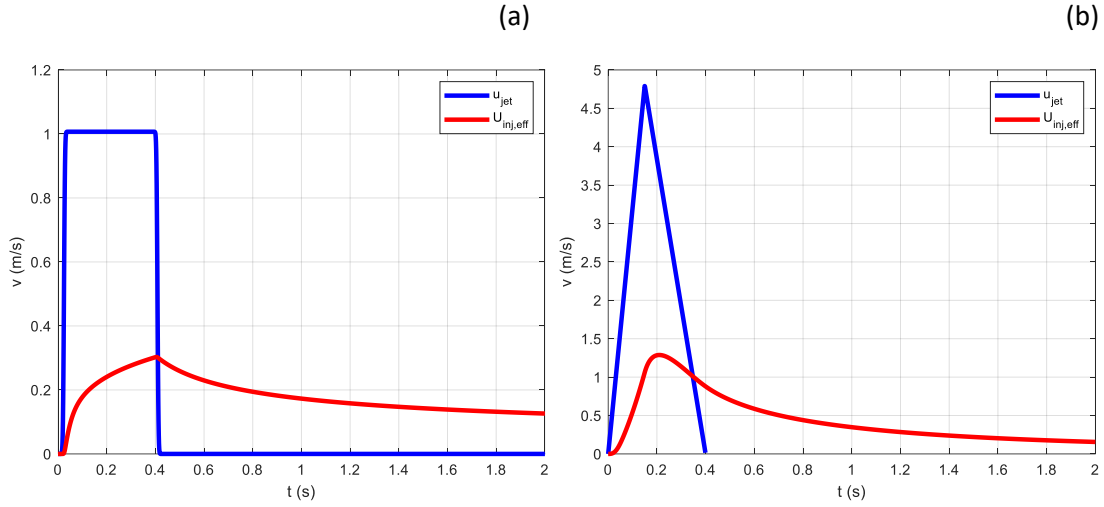

Figure 2. Time evolutions of the exit jet velocity and the effective injection velocity (Eq. 4) for conditions of (a) Experiment I of Bourouiba et al.[5] and (b) the DNS of Fabregat et al.[6]

Figure 2 shows the time evolutions of the exit velocity of the jet and the effective injection velocity for cases indicated in Table 2 for $St = 3$ and $K = 0.24$. The effective injection velocity was slightly delayed with respect to the exit jet velocity and that the maximum value was damped by approximately 70%. The effective injection velocity exhibits a monotonic decay well after the end of the jet velocity.

Dimensions of the cloud predicted by the DNS of Fabregat et al.[6] were determined from the time evolution of positions of small particles. As examples, Figures 3.a-1 and 3.b-1 show lateral views of positions of smallest particles (4 μm) and largest particles (32 μm) that stay afloat within the expelled cloud at two different times ($t = 0.6\ s$ and $t = 1.68\ s$) well after the flow injection ceased (see Fig. 2.b). The corresponding frontal views, at the same time, are plotted in Figures 4.a-1 and 4.a-2. As sketched in Fig. 1 these frontal views of the cloud have ellipsoidal shapes. Histograms of the number of particles at each axial, x, (Figs. 3.a-2 and 3.b-2), vertical, y, (Figs. 4.a-2 and 4.b-2) and spanwise, z, positions (Figs. 4.a-3 and 4.b-3) are also included. Smallest particles (4 μm) would populate preferentially the frontal part of the cloud while

particles of 32 μm are located in the rear part of the cloud. The time evolution of the position of the neck of the cloud, located between the frontal puff and the conical cloud, was obtained from the axial location where the local minimum particle concentration occurs, as illustrated in Figs. 3.a-2 and 3.b-2. The maximum diameters of the conical cloud, D_{cv} and D_{ch}, were determined from the vertical (Figs. 4.a-2 and 4.b-2) and horizontal (Figs. 4.a-3 and 4.b-3) extensions of the frontal views. Histograms of the vertical position of particles (Figs. 4.a-2 and 4.b-2) that the larger particles (32 μm) are located on average at lower vertical positions than the smallest particles (4 μm) due to the effect of gravity. In contrast, differences in the vertical distribution between particle sizes are small.

The measured time evolution of the axial position of the neck and the vertical diameter of the puff are shown in Figure 5 with symbols. The model prediction of the position of the neck using Eqs. 4 and 5 is plotted with continuous line. Similarly, to Eq. 11, the vertical and horizontal diameters of the conical cloud were determined using equation 20.

$$D_{cv}(t) = \frac{2\,x_n(t)}{n_{jv}};\; D_{ch}(t) = \frac{2\,x_n(t)}{n_{jh}} \tag{20}$$

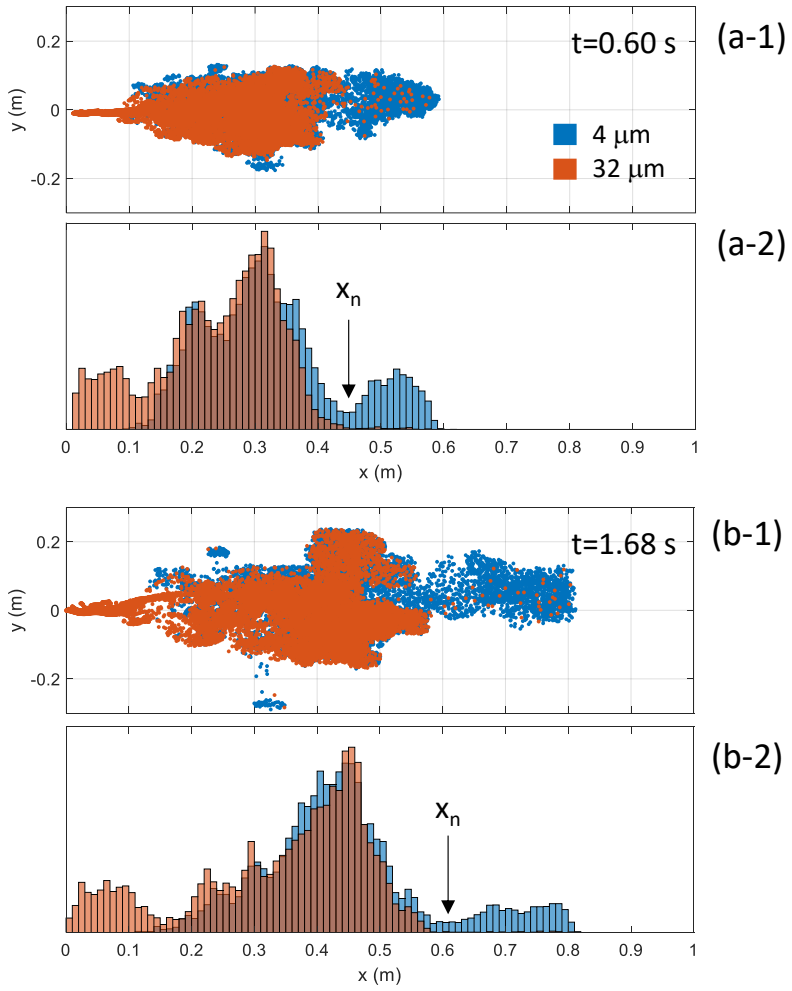

Figure 3. Lateral views of positions of particles of 4 μm (a-1) and 32 μm (b-1) at two different times. (a-2) and (b-2) Histograms of the axial position of particles.

The model reproduces well time evolutions of these two geometrical properties of the conical cloud (x_n and D_c) using the value of the Strouhal number recommended by Abani and Reitz,[43] $St = 3$. Values of spread constants in Eq. 20 that fit well numerical results are $n_{jv} = 3.3$, for the vertical diameter and $n_{jh} = 5.0$ for the horizontal diameter. While the spread constant for the horizontal diameter agrees with the value reported in the literature for jets,[10] the spread constant for the vertical diameter is significantly smaller because buoyancy would enhance the mixing along this direction.

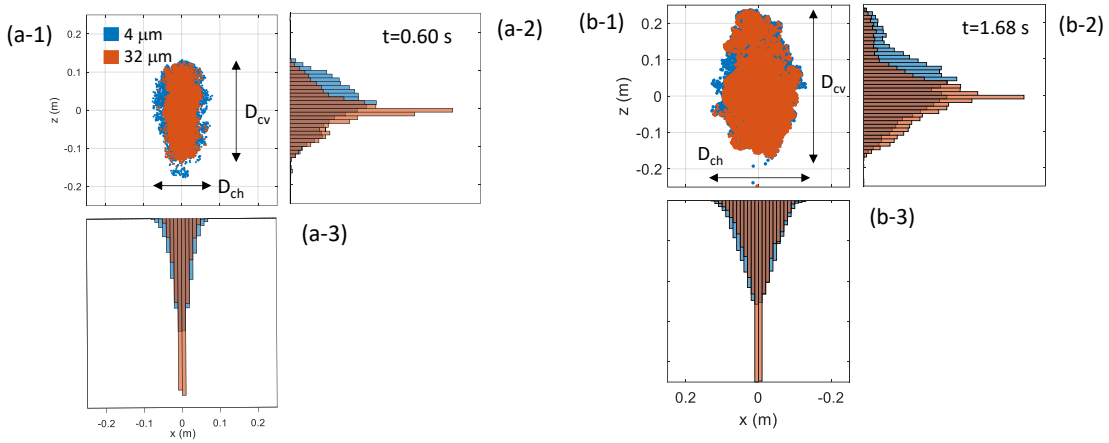

Figure 4. Frontal views of positions of particles of 4 μm (a-1) and 32 μm (b-1) at two different times. (a-2) and (b-2) Histograms of the vertical position of particles. (a-3) and (b-3) Histograms of the spanwise position of particles.

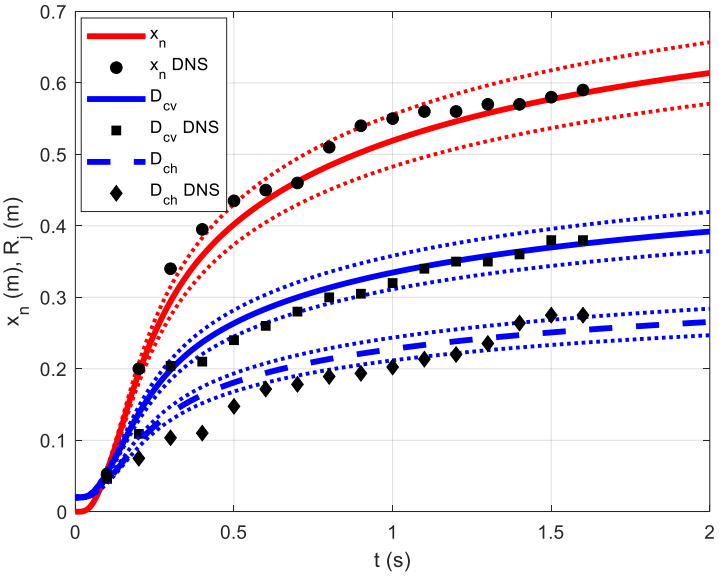

Figure 5. Time evolutions of the axial position of the neck of the cloud and it vertical and horizontal diameters. Symbols correspond to DNS of Fabregat et al.[6] and lines to the theoretical predictions with $St = 3$, $n_{jv} = 3.3$ and $n_{jh} = 5.0$. Dotted lines correspond to $\pm 7\%$ of the theoretical value.

The prediction of the lateral view of the envelope of the cloud at $t = 1.68\ s$, together with the particle positions of DNS is shown in Figure 6. Particles within the cloud are plotted in gray and particles within the frontal puff, located at, $x > 0.6\ m$, in black. Figure 6 shows that the

predicted envelope covers most of the particles within the cloud. Some parts of the cloud preferentially located on the top shear layer are out of the cone and occasional small protuberances, with ejections of a small number of particles, extend beyond the cone as shown in Fig. 6.a at positions $x \approx 0.25\ m, y \approx 0.17\ m$ and $x \approx 0.33\ m, y \approx -0.28\ m$.

The lateral view of the cone for conditions of the experiment of Bourouiba et at.[5] is shown in Fig. 7, using same parameters as for the DNS ($St = 3$, $n_{jv} = 3.3$). In this case the frontal view is not available and only the vertical extension of the cloud can be compared with the experiment. The cone covers well the extension of the dyed cloud and that the axial position of the neck is also well reproduced by the model.

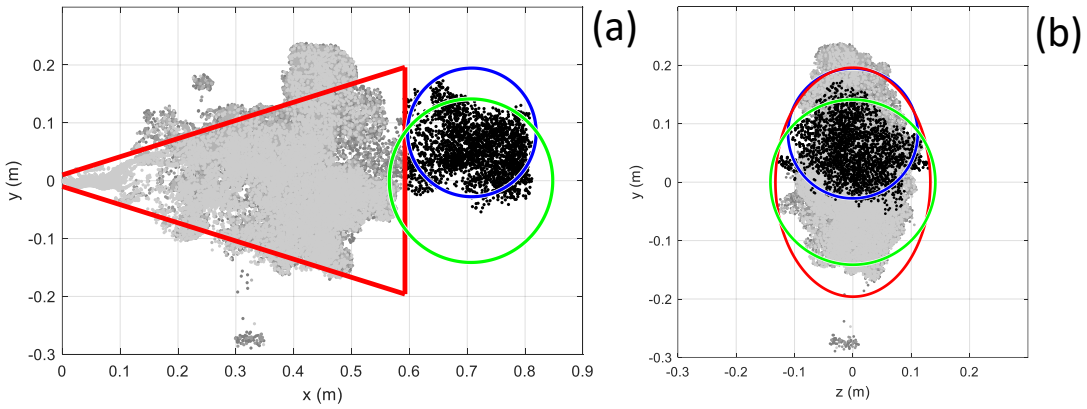

Figure 6. (a) Lateral and (b) frontal views of positions of particles predicted by the DNS of Fabregat et al.[5] at $t = 1.68\ s$. Particles within the puff are plotted in black. Red line: prediction of the envelope of the cloud with the model given in Eqs. 4, 5 and 20. Blue and green lines: positions and sizes of the puff according to the models of Richards[41] (Eqs. 12-19) and Chaudhuri et al.[44] (Eqs. 6-11), respectively.

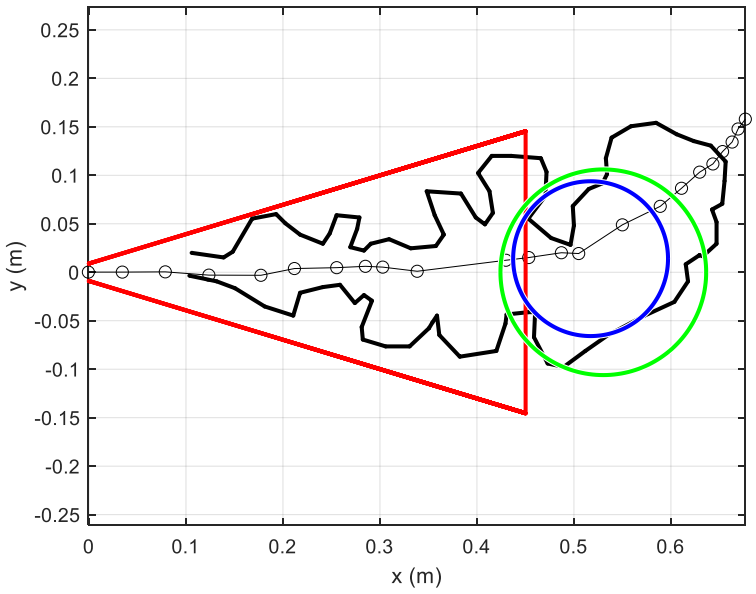

Figure 7. Black line: Lateral view of the instantaneous boundary of the dyed cloud at $t = 3.5\ s$ of Experiment I of Bourouiba et al.[5] extracted from their Fig. 10. Symbols: Trajectory of the puff extracted from Fig. 11 of Bourouiba et al.[5] Red line: prediction of the envelope of the cloud with the model given in Eqs. 4, 5 and 20. Blue line and the green lines: positions and sizes of the puff according to the models of Richards[41] (Eqs. 12-19) and Chaudhuri et al.[44] (Eqs. 6-11), respectively.

Predictions of the location and the size of the frontal puff were obtained with the model of Richards[45] and Chaudhuri et al.[44] and these are plotted in Figs. 6 and 7 with blue and green lines, respectively. For both cases, DNS and experiment, we used the same set of parameters. For the model of Richards,[45] $\eta = 3$ and $\alpha = 0.17$ and for the model of Chaudhuri et al.[44] $K = 0.457$, $n_j = n_p = 5$, which are within the ranges reported in the literature. Figures 6 and 7 show that the model of Richards[45] correctly predicts the position and the size of the puff, while the model of Chaudhuri et al.[44] does not reproduce the vertical displacement of the puff because it does not consider the buoyancy effect.

To illustrate the model implementation, Figure 8 summarizes the main steps and equations used to obtain the sizes and positions of the cloud and puff, indicated on the right part of the figure, from the input physical variables, shown on the left. The different model parameters are also included in Figure 8.

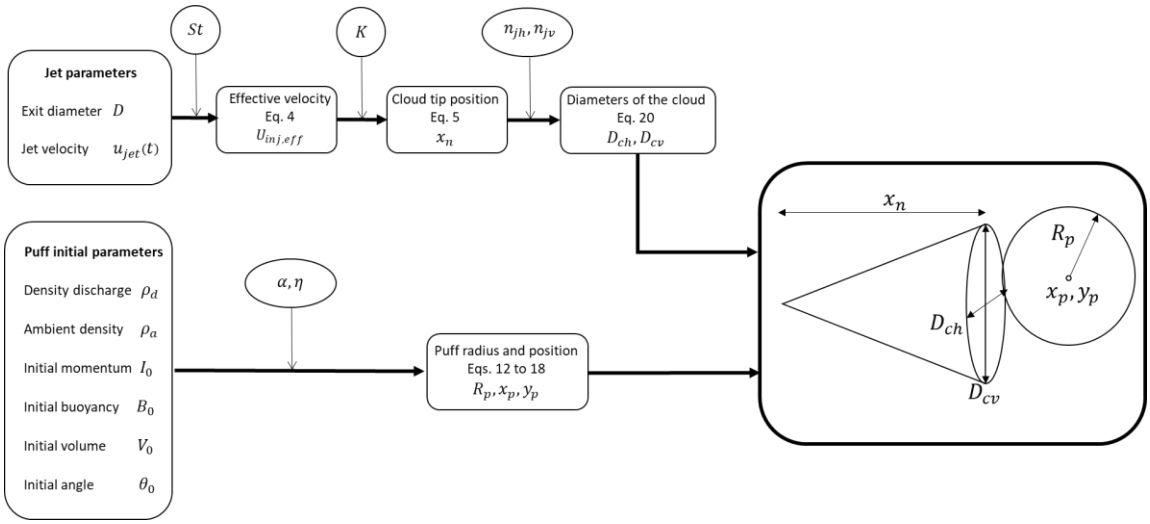

Figure 8. Steps, parameters and equations of the model.

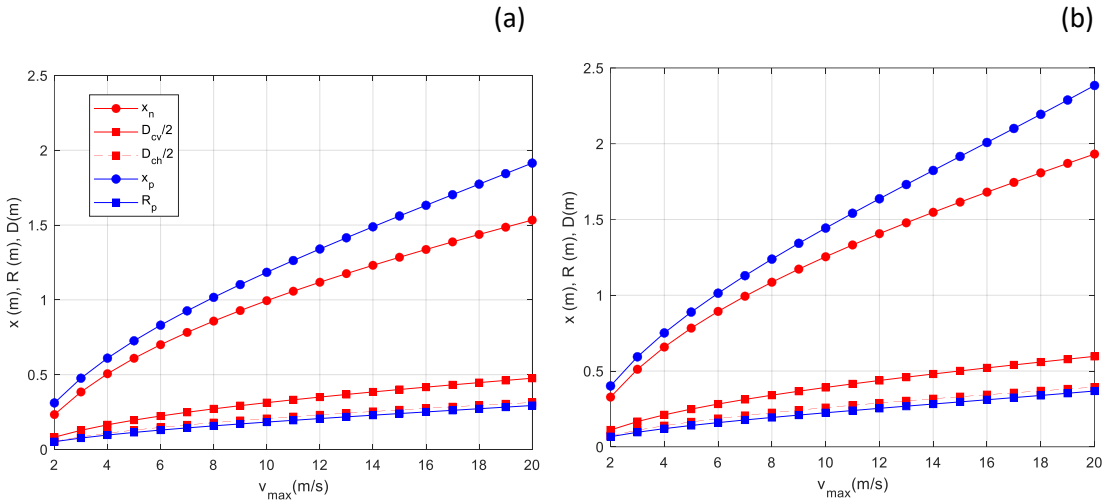

Figure 9. Dimensions and positions of the terminal cloud and puff for different maximum velocities, $u_{jet,max}$, and two injection durations. (a) $t_j = 0.4\ s$. (b) $t_j = 0.6\ s$.

To complete the discussion, in Figure 9 we plotted the prediction of dimensions and positions of the cloud and the puff for different maximum velocities and for two injection durations according to the model of the cloud shape based on the effective jet velocity and the model of puff trajectory and volume of Richards.[45] The rest of the conditions correspond to the DNS indicated in Table 2. Values of the model parameters are the same as those used for the comparison with DNS and experiments ($St = 3$, $n_{jv} = 3.3$, $n_{jh} = 5.0$, $\eta = 3$ and $\alpha = 0.17$). According to Fig. 9, the maximum range of aerosol clouds generated in mild or intense respiratory events, with maximum velocities of 10 m/s, may reach distances, $(x_p + R_p)$, of about 1.6 m, while extremely violent events with maximum velocities of 20 m/s may reach distances up to 2.8 m. For these two cases, the corresponding maximum vertical diameters of the clouds are 1.0 and 1.2 m, respectively. These distances and sizes correspond to respiratory events associated with direct and free flow injections into a quiescent ambient. It should be emphasized that these ranges and sizes are proper estimates and show the relatively large variability depending on the intensity and duration of the flow injection. Under this context, the use of face masks significantly reduces the extension and the range of the cloud as shown in experiments[23] and numerical simulations.[52] For example, Verma et al.[23] reported a reduction of the range by a factor of approximately 10.

CONCLUSIONS

In this study we derived a comprehensive model to determine the shape and dimensions of the cloud generated in violent expiratory events by combining analytical predictions of the behaviour of unsteady jet flows and puffs. Remarkably same set of values of the model parameters worked well for the two very different flow conditions considered for the validation, namely a mild cough (DNS by Fabregat et al.[6]) and a sneeze (experiment by Bourouiba et al.[5]). Despite significantly distinct values of momentum and buoyancy inlet fluxes, the model can be used to predict readily and accurately the short-term dispersion of a wide range of expiratory events.

The model, based on dynamics of jets with unsteady flow injection and buoyant puffs, allows to predict the short-term envelope of the aerosol cloud generated in an intense or violent respiratory event. In these quasi-instantaneous events, with a typical duration of half a second, droplets of different sizes are expelled at relatively large velocities. While large droplets reach the floor following quasi-ballistic trajectories soon after the release, small droplets and droplet nuclei, constituted by the non-evaporable residual of saliva and sputum, stay afloat within the decaying turbulent cloud produced by the flow injection. This cloud exhibits a quasi-conical shape and at the frontal part a puff is formed. A few seconds after the flow injection has ceased velocities within the cloud and the puff reach typical values of background velocities in forced or naturally ventilated spaces. The subsequent long-term dispersion of this aerosol in these spaces has typical time scales of one or two orders of magnitude larger than the time scale associated with the formation and decay of the aerosol cloud and puff.

The model reproduces well the overall characteristics of the envelope of these clouds and puffs of experimental visualizations and Direct Numerical Simulations reported in the literature. Specifically, a model based on dynamics of jets with unsteady flow injection provides reasonable estimates of the observed conical envelope of the aerosol cloud for the relatively different conditions of experiments and simulations. If the exhaled air flow has a lower density than the ambient typically around 20°C, as it occurs in real expiratory events with exhalation temperatures close to 37°C, buoyancy causes different entrainment rates along the vertical and spanwise directions. As a result, the cloud exhibits elliptical cross sections, with the major axis aligned with the vertical direction and the minor axis with the spanwise direction. Dimensions and the location of the frontal quasi-spherical puff are well reproduced by a model based on the mass and momentum conservation equations.

When velocities of the cloud have reached typical ambient background velocities, the model predicts maximum ranges of aerosol clouds and puffs of about 1.6 m for intense respiratory events with maximum velocities of 10 m/s. The distance is increased up to 2.8 m for violent events with maximum velocities of 20 m/s. The position and the shape of the cloud and the puff obtained with the model can be used to establish initial conditions for simulations of the long-term dispersion in enclosed spaces.

Authors' contribution

All authors contributed equally in the preparation of this manuscript.

Declaration of conflicting interests

The authors declared no potential conflicts of interest with respect to the research, authorship, and/or publication of this article

Funding

This work has been funded by Spanish Ministerio de Ciencia, Innovación y Universidades through the grants PID2020-113303GB-C21 and RTI2018-100907-A-I00 (MCIU/AEI/FEDER) and by the Generalitat de Catalunya through the grant 2017-SGR-1234.

REFERENCES

1. Jones R M and Brosseau L M. Aerosol transmission of infectious disease. *Journal of Occupational and Environmental Medicine* 2015; 57(5): 501-508.

2. Asadi S, Bouvier N, Wexler A S and Ristenpart W D. The coronavirus pandemic and aerosols: Does COVID-19 transmit via expiratory particles? *Aerosol Science and Technology* 2020; 54(6): 635-638.

3. Bourouiba L. The fluid dynamics of disease transmission. *Annual Review of Fluid Mechanics* 2021; 53: 473-508.

4. Mittal R, Ni R and Seo J H. The flow physics of COVID-19. *Journal of Fluid Mechanics* 10 July 2020; 894, F2. https://doi.org/10.1017/jfm.2020.330

5. Bourouiba L, Dehandschoewercker E and Bush J W. Violent expiratory events: on coughing and sneezing. *Journal of Fluid Mechanics* 2014; 745: 537-563.

6. Fabregat A, Gisbert F, Vernet A, Ferré J A, Mittal K, Dutta S and Pallares J. Direct numerical simulation of turbulent dispersion of evaporative aerosol clouds produced by an intense expiratory event. *Physics of Fluids* 2021; 33: 033329.

7. Dbouk T and Drikakis D. Weather impact on airborne coronavirus survival. *Physics of Fluids* 2020; 32(9): 093312.

8. Nicas M, Nazaroff W W and Hubbard A. Toward understanding the risk of secondary airborne infection: emission of respirable pathogens. *Journal of Occupational and Environmental Hygiene* 2005; 2(3): 143-154.

9. Stadnytskyi V, Bax C E, Bax A and Anfinrud P. The airborne lifetime of small speech droplets and their potential importance in SARS-CoV-2 transmission. *Proceedings of the National Academy of Sciences* 2020; 117(22): 11875-11877.
10. Scorer R S. *Dynamics of meteorology and climate*. 1st ed. Wiley, New York, 1997.
11. Khalafvand S S, Xu F, Westenberg J, Gijsen F and Kenjeres S. Intraventricular blood flow with a fully dynamic mitral valve model. *Computers in Biology and Medicine* 2019; 104: 197-204.
12. Anderson E J and Grosenbaugh M A. Jet flow in steadily swimming adult squid. *Journal of Experimental Biology* 2005; 208(6): 1125-1146.
13. Abraham J. Entrainment characteristics of transient gas jets. *Numerical Heat Transfer Part A Applications* 1996; 30(4): 347-364.
14. Gupta J K, Lin C H and Chen Q. Flow dynamics and characterization of a cough. *Indoor air* 2009; 19(6): 517-525.
15. Busco G, Yang S R, Seo J and Hassan Y A. Sneezing and asymptomatic virus transmission. *Physics of Fluids* 2020; 32(7): 073309.
16. Mansour E, Vishinkin R, Rihet S, Saliba W, Fish F, Sarfati P and Haick H. Measurement of temperature and relative humidity in exhaled breath. *Sensors and Actuators B: Chemical* 2020; 304: 127371.
17. Duguid J P. The size and the duration of air-carriage of respiratory droplets and droplet nuclei. *Epidemiology and Infection* 1946; 44(6): 471-479.
18. Zayas G, Chiang M C, Wong E, MacDonald F, Lange C F, Senthilselvan A and King M. Cough aerosol in healthy participants: fundamental knowledge to optimize droplet-spread infectious respiratory disease management. *BMC Pulmonary Medicine* 2012; 12(1): 1-12.
19. Han Z Y, Weng W G and Huang Q Y. Characterizations of particle size distribution of the droplets exhaled by sneeze. *Journal of the Royal Society Interface* 2013; 10(88): 20130560.
20. Lee J, Yoo D, Ryu S, Ham S, Lee K, Yeo M, Min K and Yoon C. Quantity, size distribution, and characteristics of cough-generated aerosol produced by patients with an upper respiratory tract infection. *Aerosol and Air Quality Research* 2019; 19(4): 840-853.
21. Creeth J M. Constituents of mucus and their separation. British medical bulletin 1978; 34(1): 17-24.
22. Arumuru V, Pasa J and Samantaray S S. Experimental visualization of sneezing and efficacy of face masks and shields. *Physics of Fluids* 2020; 32(11): 115129.
23. Verma S, Dhanak M and Frankenfield J. Visualizing the effectiveness of face masks in obstructing respiratory jets. *Physics of Fluids* 2020; 32(6): 061708.

24. Gupta J K, Lin C H and Chen Q. Transport of expiratory droplets in an aircraft cabin. *Indoor Air* 2011; 21(1): 3-11.
25. Thatiparti D S, Ghia U and Mead K R. Computational fluid dynamics study on the influence of an alternate ventilation configuration on the possible flow path of infectious cough aerosols in a mock airborne infection isolation room. *Science and Technology for the Built Environment* 2017; 23(2): 355-366.
26. Yang L, Li X, Yan Y and Tu J. Effects of cough-jet on airflow and contaminant transport in an airliner cabin section. *The Journal of Computational Multiphase Flows* 2018; 10(2): 72-82.
27. Nazari A, Jafari M, Rezaei N, Taghizadeh-Hesary F and Taghizadeh-Hesary F. Jet fans in the underground car parking areas and virus transmission. *Physics of Fluids* 2021; 33(1): 013603.
28. Yu H C, Mui K W and Wong L T. Numerical simulation of bioaerosol particle exposure assessment in office environment from MVAC systems. *The Journal of Computational Multiphase Flows* 2018; 10(2): 59-71.
29. Dbouk T and Drikakis D. On coughing and airborne droplet transmission to humans. *Physics of Fluids* 2020; 32(5): 053310.
30. Diwan S S, Ravichandran S, Govindarajan R and Narasimha R. Understanding transmission dynamics of COVID-19-type infections by direct numerical simulations of cough/sneeze flows. *Transactions of the Indian National Academy of Engineering* 2020; 5: 255-261.
31. Pendar M R and Páscoa J C. Numerical modeling of the distribution of virus carrying saliva droplets during sneeze and cough. *Physics of Fluids* 2020; 32(8): 083305.
32. Shao X and Li X. COVID-19 transmission in the first presidential debate in 2020. *Physics of Fluids* 2020; 32(11): 115125.
33. Zhang Z, Han T, Yoo K H, Capecelatro J, Boehman A L and Maki K. Disease transmission through expiratory aerosols on an urban bus. *Physics of Fluids* 2021; 33(1): 015116.
34. Dbouk T and Drikakis D. On airborne virus transmission in elevators and confined spaces. *Physics of Fluids* 2021; 33(1): 011905.
35. Liu H, He S, Shen L and Hong J. Simulation-based study of COVID-19 outbreak associated with air-conditioning in a restaurant. *Physics of Fluids* 2021; 33(2): 023301.
36. Fontes D, Reyes J, Ahmed K and Kinzel M. A study of fluid dynamics and human physiology factors driving droplet dispersion from a human sneeze. *Physics of Fluids* 2020; 32(11): 111904.
37. Foster A and Kinzel M. Estimating COVID-19 exposure in a classroom setting: A comparison between mathematical and numerical models. *Physics of Fluids* 2021; 33(2): 021904.
38. Cravero C and Marsano D. Simulation of COVID-19 indoor emissions from coughing and breathing with air conditioning and mask protection effects. *Indoor and Built Environment, epubl ahead of print,* 24 August 2021; doi:10.1177/1420326X211039546.

39. Abkarian M, Mendez S, Xue N, Yang F and Stone H A. Speech can produce jet-like transport relevant to asymptomatic spreading of virus. *Proceedings of the National Academy of Sciences* 2020; 117(41): 25237-25245.

40. Wang J, Alipour M, Soligo G, Roccon A, De Paoli M, Picano F and Soldati A. Short-range exposure to airborne virus transmission and current guidelines. *Proceedings of the National Academy of Sciences* 2021; 118(37): e2105279118.

41. Richards J M. Inclined buoyant puffs. *Journal of Fluid Mechanics* 1968; 32(4):681-692.

42. Schlichting H and Gersten K. *Boundary layer theory*, Springer, Berlin, 2017.

43. Abani N and Reitz, R D. Unsteady turbulent round jets and vortex motion. *Physics of Fluids* 2007; 19(12): 125102.

44. Chaudhuri S, Basu S, Kabi P, Unni V R and Saha A. Modeling the role of respiratory droplets in Covid-19 type pandemics. *Physics of Fluids* 2020; 32(6): 063309.

45. Richards J M. Puff motions in unstratified surroundings. *Journal of Fluid Mechanics* 1965; 21(1): 97-106.

46. Renzi E and Clarke A. Life of a droplet: Buoyant vortex dynamics drives the fate of micro-particle expiratory ejecta. *Physics of Fluids* 2020; 32(12): 123301.

47. Scorer R S. Experiments on convection of isolated masses of buoyant fluid. *Journal of Fluid Mechanics* 1957; 2(6): 583-594.

48. Fabregat A, Gisbert F, Vernet A, Mittal K, Dutta S and Pallares J. Direct numerical simulation of the turbulent flow generated during a violent expiratory event. *Physics of Fluids* 2021; 33: 035122.

49. Chong K L, Ng C S, Hori N, Yang R, Verzicco R and Lohse D. Extended lifetime of respiratory droplets in a turbulent vapor puff and its implications on airborne disease transmission. *Physical Review Letters* 2021; 126(3): 034502.

50. Wang J, Dalla Barba F and Picano F. Direct numerical simulation of an evaporating turbulent diluted jet-spray at moderate Reynolds number. *International Journal of Multiphase Flow* 2021; 137: 103567.

51. Dalla Barba F and Picano F. Clustering and entrainment effects on the evaporation of dilute droplets in a turbulent jet. *Physical Review Fluids* 2018; 3(3): 034304.

52. Dbouk T and Drikakis D. On respiratory droplets and face masks. *Physics of Fluids* 2020; 32(6): 063303.